Aluminum and boron nuclear quadrupole resonance with a direct current superconducting quantum interference device

C. Connor,[a] J. Chang, and A. Pines
Materials and Chemical Sciences Division, Lawrence Berkeley Laboratory, and Department of Chemistry, University of California, Berkeley, California 94720

(Received 31 May 1990; accepted 28 August 1990)

We report the application of our dc SQUID (superconducting quantum interference device) spectrometer [C. Connor, J. Chang, and A. Pines, Rev. Sci. Instrum. **61**, 1059(1990)] to nuclear quadrupole resonance (NQR) studies of aluminum-27, and boron-11 in crystalline and glassy solids. Our results give $e^2qQ/h = 2.38$ MHz and $\eta = 0.0$ for α–Al_2O_3 at 4.2 K. For the natural mineral petalite ($LiAlSi_4O_{10}$), we obtain $e^2qQ/h = 4.56$ MHz and $\eta = 0.47$. The quadrupole resonance frequency is 1467 kHz in boron nitride, and in the vicinity of 1300 kHz for various borates in the $B_2O_3 \cdot xH_2O$ system. The distribution of boron environments in a B_2O_3 glass gives rise to a linewidth of about 80 kHz in the SQUID detected resonance.

I. INTRODUCTION

Nuclear quadrupole resonance spectroscopy (NQR) is an excellent method to probe chemical bonds, and the environment of an atomic nucleus, because the electric field gradients at the nucleus arise primarily from valence electrons.[1,2] In this paper we report the measurement of NQR spectra by monitoring the magnetization induced in a sample, during a radiofrequency (rf) sweep, by means of a dc superconducting quantum interference device (SQUID). The technique is a broadband method for measuring quadrupole resonances from a few hundred kilohertz to tens of megahertz. Single crystal or polycrystalline samples may be used to determine accurate values for the quadrupole splitting, with minimal line broadening.

In high field NMR of polycrystalline samples, the random distribution of crystal axis orientations with respect to the applied magnetic field produces a broad powder spectrum. For quadrupolar nuclei with noninteger spin, one usually observes only the central ($+1/2 \leftrightarrow -1/2$) transition, and information about the quadrupolar interaction must be extracted from this transition. This is often done by numerical simulations of the spectra, sometimes in combination with magic-angle spinning (MAS).[3,4] Recent progress, using the novel methods of dynamic-angle spinning (DAS) and double rotation (DOR), has allowed for high-resolution spectra providing a more direct way of deriving NQR data on the sample.[5]

When the quadrupole splittings are large, pure NQR can be used, but for small splittings conventional NQR spectrometers are not useful because the signals associated with the low frequencies are weak. This is the case for a number of important isotopes, including ^{2}D, ^{7}Li, ^{11}B, ^{17}O, ^{23}Na, and ^{27}Al, which often have resonance frequencies below a few megahertz. The techniques of field cycling and indirect detection have been applied to obtain low and zero field spectra,[6] but it would be desirable to detect the signals directly.

Such direct low frequency measurements of NQR transitions are possible using a dc SQUID,[7] a device which directly measures the magnetic flux from the sample. The dc SQUID itself is capable of detecting signals over a frequency range from dc to tens of megahertz, since its sensitivity is relatively independent of the frequency of the oscillating magnetization. However, a flux-locked dc SQUID, which provides a linear response to the sample magnetization, can typically operate only from dc to a few hundred kilohertz. This frequency limitation is due to the feedback circuit used for flux-locking. We have taken advantage of the linear response of the flux-locked dc SQUID, while avoiding the frequency limitations of the feedback circuit, by measuring longitudinal (z-axis) magnetization rather than transverse magnetization. This approach was originally demonstrated with an rf SQUID.[8] In this paper, an extension of our previous communication on ^{27}Al in α–Al_2O_3,[9] we present a detailed description of the technique, and further results on the NQR of ^{27}Al and ^{11}B in crystalline and glassy solids.

II. ZERO FIELD NQR WITH DETECTION OF LONGITUDINAL MAGNETIZATION

The spin Hamiltonian for a quadrupolar nucleus in a low magnetic field is given by

$$H = H_Q + H_Z + H_D. \tag{1}$$

The dominant term is the quadrupolar Hamiltonian,[2] written as

$$H_Q = -\frac{e^2qQ}{4\hbar\mathbf{I}(2\mathbf{I}-1)}\left[3\mathbf{I}_z^2 - \mathbf{I}^2 + \eta(\mathbf{I}_x^2 - \mathbf{I}_y^2)\right] \tag{2}$$

when expressed in the principal axis system (PAS) of the quadrupolar interaction. The second term is the magnetic Zeeman Hamiltonian,

$$H_Z = -\gamma\hbar B_o(I_z\cos\theta + I_x\sin\theta\cos\phi + I_y\sin\theta\sin\phi), \tag{3}$$

where θ and ϕ define the orientation of the magnetic field with respect to the PAS of the quadrupolar interaction and γ is the gyromagnetic ratio of the nucleus. The last term is the

[a] Present address: Defence Research Establishment Pacific, CFB Esquimalt, FMO Victoria, B.C., V0S 1B0, Canada.

dipole–dipole Hamiltonian, which appears only as a small perturbation on the quadrupolar interaction and will not be discussed in detail. Our treatment is limited to nuclei with noninteger spin in an axially symmetric electric field gradient.

A. Single crystal sample

The energy level scheme of a spin with $\mathbf{I} = 3/2$ is shown in Fig. 1. In zero magnetic field, there is only one transition, the pure quadrupolar resonance, at $\omega_Q = e^2qQ/2\hbar$. Applying a small magnetic field parallel to the z-axis of the quadrupolar PAS splits the degeneracy of the levels, resulting in two transitions, at $\omega_{Q,+m} = \omega_Q - \gamma B_0$ and $\omega_{Q,-m} = \omega_Q + \gamma B_0$, centered about ω_Q.[10] At thermal equilibrium the spin states have, according to the high temperature approximation, the following relative populations:

$$P_{+3/2} = \frac{1}{4}\left(1 - \frac{e^2qQ}{4kT} + \frac{3\gamma\hbar B_0}{2kT}\right), \tag{4a}$$

$$P_{-3/2} = \frac{1}{4}\left(1 - \frac{e^2qQ}{4kT} - \frac{3\gamma\hbar B_0}{2kT}\right), \tag{4b}$$

$$P_{+1/2} = \frac{1}{4}\left(1 + \frac{e^2qQ}{4kT} + \frac{\gamma\hbar B_0}{2kT}\right), \tag{4c}$$

$$P_{-1/2} = \frac{1}{4}\left(1 + \frac{e^2qQ}{4kT} - \frac{\gamma\hbar B_0}{2kT}\right). \tag{4d}$$

Using

$$M_Z = N\gamma\hbar \sum_m mP_m, \tag{5}$$

where N is the number density of spins, the net magnetization of the sample is

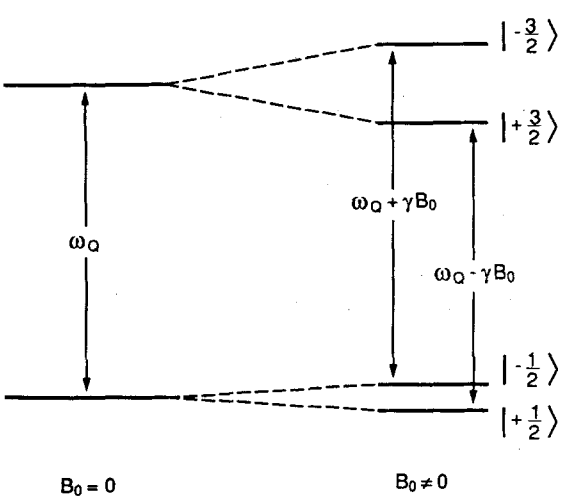

FIG. 1. Energy levels for a spin $\mathbf{I} = 3/2$ with a small magnetic field ($\gamma B_0 \ll e^2qQ/\hbar$) along the z-axis of the electric field gradient. During a sweep from low to high frequency, one rotating component of the linearly polarized rf excites transitions between the $+3/2$ and $+1/2$ states, inducing a net magnetization in the sample. As the frequency sweep continues, the counter-rotating component of the rf destroys the magnetization by exciting transitions between the $-3/2$ and $-1/2$ states. During the sweep, the z-axis magnetization of the sample is monitored by a dc SQUID.

$$M_Z = \frac{N\gamma\hbar^2}{4kT}\left[\frac{10}{2}\gamma B_0\right]. \tag{6}$$

Consider the effect of a linearly polarized rf field swept through the two components of the $\pm 1/2 \leftrightarrow \pm 3/2$ transition. The linearly polarized rf can be decomposed into two counter-rotating fields, left circularly polarized and right circularly polarized. Each rf component selectively excites transitions within either the $+m$ or the $-m$ manifold.[11] During a sweep of saturating linearly polarized rf from low to high frequency, the populations of the $+3/2$ and $+1/2$ states are equalized by one component of the rf, giving the new populations

$$P'_{+3/2} = P'_{+1/2} = \frac{1}{4}\left(1 + \frac{\gamma\hbar B_0}{kT}\right). \tag{7}$$

After saturating this $+3/2 \leftrightarrow +1/2$ component, the sample magnetization is

$$M'_Z = \frac{N\gamma\hbar^2}{4kT}\left[\frac{9}{2}\gamma B_0 + \frac{1}{4}\frac{e^2qQ}{\hbar}\right]. \tag{8}$$

A comparison of Eq. (8) with Eq. (6) shows that saturating the $+3/2 \leftrightarrow +1/2$ component produces a large increase in the sample magnetization, when $e^2qQ/\hbar \gg \gamma B_0$. This induced magnetization will remain, neglecting relaxation processes, until the $-m$ manifold is excited. As the sweep is continued, the other component of the rf saturates the $-3/2 \leftrightarrow -1/2$ component of the transition, reducing the magnetization to

$$M''_Z = \frac{N\gamma\hbar^2}{4kT}\left[\frac{8}{2}\gamma B_0\right], \tag{9}$$

close to its original value.

For $\mathbf{I} = 5/2$ nuclei, the initial magnetization is

$$M_Z = \frac{N\gamma\hbar^2}{6kT}\left[\frac{35}{2}\gamma B_0\right]. \tag{10}$$

The induced magnetization becomes

$$M'_Z = \frac{N\gamma\hbar^2}{6kT}\left[17\gamma B_0 + \frac{3}{40}\frac{e^2qQ}{\hbar}\right], \tag{11}$$

when exciting the $\pm 1/2 \leftrightarrow \pm 3/2$ transition, and

$$M'_Z = \frac{N\gamma\hbar^2}{6kT}\left[17\gamma B_0 + \frac{6}{40}\frac{e^2qQ}{\hbar}\right], \tag{12}$$

when exciting the $\pm 3/2 \leftrightarrow \pm 5/2$ transition. The final magnetization, when exciting either the $\pm 1/2 \leftrightarrow \pm 3/2$ or the $\pm 3/2 \leftrightarrow \pm 5/2$ transition, is

$$M''_Z = \frac{N\gamma\hbar^2}{6kT}\left[\frac{33}{2}\gamma B_0\right]. \tag{13}$$

A few modifications to the above equations need to be made when considering a sweep from high to low frequency. Since the order in which the two components of the transition are saturated is reversed, the sign of the quadrupolar term in Eqs. (8), (11), and (12) must be changed. The sign of the Zeeman terms remains the same. Since the magnitude of the quadrupolar term is normally much larger than that of the Zeeman term, the sign of the resonance peak is effectively switched. This behavior provides a convenient means to distinguish between instrumental artifacts and NQR signals.

Although the above equations predict a single square

wave signal, in practice several other factors must be considered when attempting to predict the observed line shape. We discuss these factors first for a single crystal sample, with an axially symmetric quadrupolar axis aligned along the dc magnetic field. In Sec. II B we extend the discussion to the $\pm m \leftrightarrow \pm (m+1)$ (for $m > 1/2$) transitions of a powder sample, and finally to the case of the $\pm 1/2 \leftrightarrow \pm 3/2$ transition of a powder sample.

The line shape for a single crystal sample, with the quadrupolar axis parallel to the magnetic field, can be approximated by

$$S(\omega) = \int_0^{\omega} [g_{+m}(\omega') + g_{-m}(\omega')] e^{-(\omega-\omega')/\kappa T_1} d\omega'. \tag{14}$$

The functions $g_{\pm m}(\omega')$ are Gaussians, centered at $\omega_Q \pm \gamma B_0$, representing the absorption line shapes of the two components contributing to the transition. If we assume the sample to be a perfect crystal, the width of each Gaussian is determined by dipolar coupling. The time constant T_1 accounts for the effects of spin–lattice relaxation during the sweep, and κ is the sweep rate. Simulated line shapes of the $\pm 3/2 \leftrightarrow \pm 5/2$ transition are compared, in Fig. 2, with those observed experimentally from an α–Al_2O_3 crystal.

Cross relaxation between the $+m$ and $-m$ manifolds may also be important in determining the line shape. After the excitation of the $+m$ manifold, and before reaching the $-m$ manifold, the spin system undergoes cross relaxation between the manifolds as well as spin–lattice relaxation. Both of these processes tend to decrease the magnitude of the induced magnetization. Cross relaxation between neighboring nuclei is induced by the $\mathbf{I}_{+i}\mathbf{I}_{+j}$ and $\mathbf{I}_{-i}\mathbf{I}_{-j}$ terms of the dipolar interaction.[12] Both of these spin–operator terms produce nearly energy-conserving spin flip–flips. One of them acts to increase the magnetization, while the other reduces the magnetization, depending on the sign of the gyromagnetic ratio and the direction of the sweep. The flip–flip which reduces the magnetization is always more probable because of the thermal equilibrium population distribution of the unperturbed transition. The rate of the frequency sweep effectively determines the amount of time that cross relaxation is allowed to occur. Cross relaxation makes it difficult to accurately predict the line shape of the resonance *a priori* and may slightly shift the position of the line towards the direction of the rf sweep. However, as explained in Sec. II C, the effect of this shift can be easily removed while recording spectra.

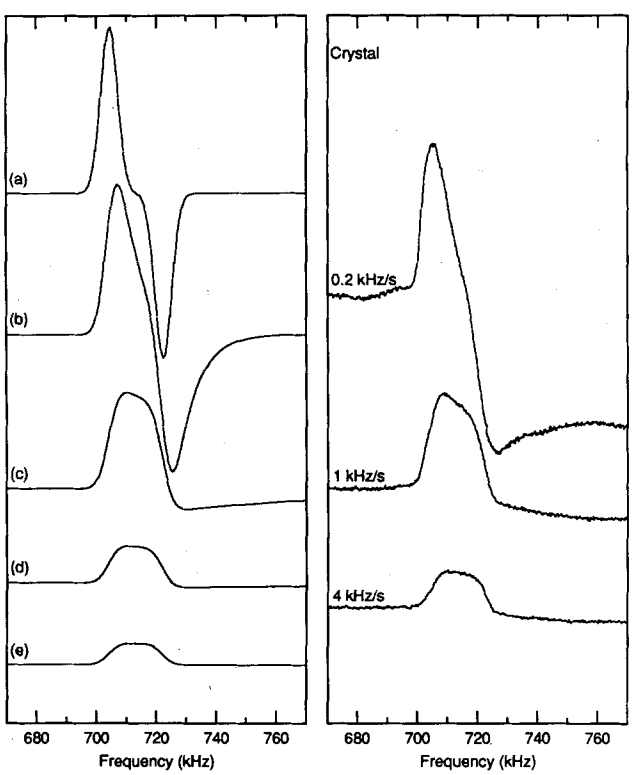

FIG. 2. Simulated (left) and experimental forward sweeps of the $\pm 3/2 \leftrightarrow \pm 5/2$ transition of an α–Al_2O_3 crystal, for various sweep rates. In Figs. 2 and 3, the amplitudes of the simulated spectra are matched to the amplitudes of the experimental spectra. The experimental signal-to-noise was increased in some cases by run-averaging. The α–Al_2O_3 spectra were obtained in a 10 G dc field at 4.2 K.

B. Unoriented samples

In powders, glasses, and amorphous samples, the z-axes of the quadrupolar principal axis systems are not uniformly aligned with respect to the dc magnetic field. The dc field is truncated by the quadrupolar interaction, becoming $B_{0,\text{eff}} = B_0 \cos\theta$, where θ is the polar angle between the field and the quadrupolar symmetry axis. For $|m| \geq 3/2$ the eigenstates are unchanged, and Eq. (14) may still be used to describe the expected line shape. However, the functions $g_{\pm m}(\omega')$ must be replaced by the corresponding powder averages,

$$g_{\pm m}(\omega', B_0, B_1) = \frac{1}{4\pi} \int_0^{2\pi} d\phi \int_0^{\pi} g_{\pm m}(\omega', \theta) \times \Psi(\theta, B_1) \Gamma(\theta) \Xi(\theta, B_0) \sin\theta \, d\theta. \tag{15}$$

In this equation $g_{\pm m}(\omega', \theta)$ are Gaussians centered at $\omega_Q \pm \gamma B_0 \cos\theta$. The width of these Gaussians is determined both by the distribution of quadrupolar coupling parameters within the sample, and by dipolar coupling between nuclei in the sample. For glassy or amorphous samples the contribution from the distribution of quadrupolar parameters may far outweigh the contribution from dipolar coupling. For highly crystalline samples, the line broadening will be exclusively due to dipolar coupling. In Sec. IV we show spectra which exhibit both these extremes. The other terms can be explained as follows.

The rf radiation is most effective in inducing transitions when it is applied orthogonally to the quadrupole symmetry axis. This will not be the case for many crystallites in a powder sample, so the $\Psi(\theta, B_1)$ term takes into account that only the projection of the rf perpendicular to the quadrupolar z-axis is effective in inducing transitions. From studies of a single crystal of α–Al_2O_3, we find that the $\Psi(\theta, B_1)$ term, which describes the signal height as a function of rf strength, has the approximate form

$$\Psi(\theta,B_1)\approx 1-\exp(-B_{1,\mathrm{eff}}/B_{1,0}). \quad (16)$$

The effective rf field is $B_{1,\mathrm{eff}}=B_1\cos\theta$, and $B_{1,0}$ is a characteristic rf strength which depends on the sample parameters and the sweep rate.

The magnetization induced in a spin system appears along the z-axis of the quadrupole PAS, while the SQUID measures magnetization along the laboratory z-axis. The detected signal from a crystallite with polar angle θ will thus be proportional to $\Gamma(\theta)\sim\cos\theta$.

The small dc field, used to split the degeneracy of the $\omega_{Q,+m}$ and $\omega_{Q,-m}$ components, reduces the cross relaxation rate between the $+m$ and $-m$ manifolds. The effective field, $B_{0,\mathrm{eff}}=B_0\cos\theta$, decreases in crystallites for which the z-axis is tilted away from the magnetic field axis. The $\Xi(\theta,B_0)$ term accounts for the decreased effectiveness of the dc field in reducing the cross relaxation rate when the quadrupolar z-axis is not aligned along the magnetic field. The result is a reduction in signal intensity, and a distortion of the line shape, when the effective field approaches the local field B_L (due to dipolar coupling) of the sample. We have found that, for a single crystal of α–Al_2O_3, $\Xi(\theta,B_0)$ can be roughly represented by

$$\Xi(\theta,B_0)\approx 1-\exp(-B_{0,\mathrm{eff}}/B_L). \quad (17)$$

The sweep rate and the zero field cross relaxation rate affect the overall magnitude of $\Xi(\theta,B_0)$. Figure 3 shows a comparison of simulated and experimental line shapes for the $\pm 3/2\leftrightarrow\pm 5/2$ transition of an α–Al_2O_3 powder.

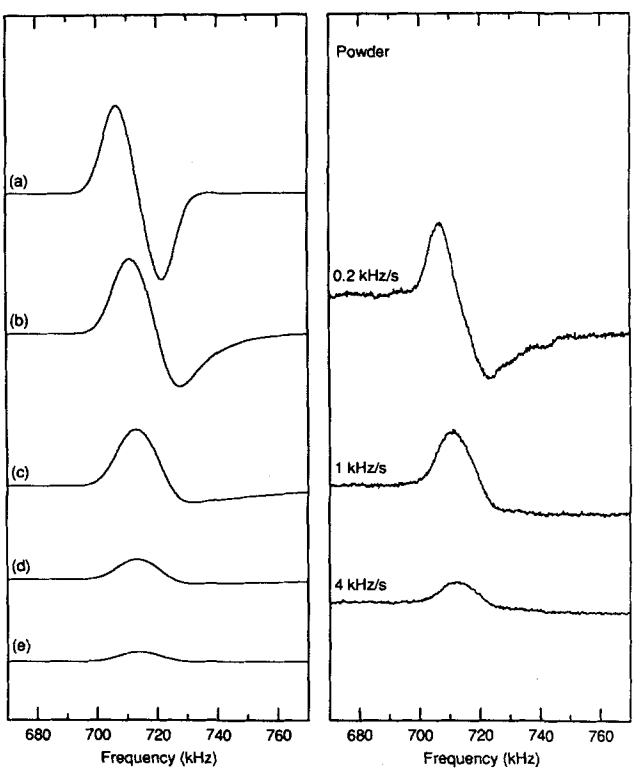

FIG. 3. Simulated (left) and experimental forward sweeps of the α–Al_2O_3 powder sample, using the $\pm 3/2\leftrightarrow\pm 5/2$ transition, for various sweep rates.

A description of the line shape of the $\pm 1/2\leftrightarrow\pm 3/2$ transition is somewhat more complicated, due to zero order mixing of the $+1/2$ and $-1/2$ states by the dc field. In this case the transition is made up of four components, so four g_i's are required in Eq. (14). The amplitude and frequency of each component have been given by Das and Hahn.[2]

Several points regarding the comparison of the powder and single crystal line shapes should be apparent from the above discussion. Consider a powder sample composed of highly crystalline particles, so the only source of line broadening is the dipolar coupling. Under optimum conditions ($B_0=B_L$, and a fast sweep), both the powder and crystal samples give roughly Gaussian lines about one and one-half times wider than the natural linewidth. For a given dc field strength, the $\pm 3/2\leftrightarrow\pm 5/2$ transition of a powder sample is slightly narrower than that of the crystal. This situation, of which an example is given in Figs. 2 and 3, may be unique in magnetic resonance. Because of the mixing of the $+1/2$ and $-1/2$ states in a powder sample, the $\pm 1/2\leftrightarrow\pm 3/2$ transition is about three times as broad as the $\pm 3/2\leftrightarrow\pm 5/2$ transition.

If the nuclei of interest in the sample experience a distribution of quadrupolar splittings, as in amorphous samples, this distribution will often determine the observed linewidth. Since the dc field need be only of comparable strength to the dipolar interaction, the line shape and linewidth observed using the SQUID NQR technique described in this paper will be similar to those observed in pure NQR. For these samples the $\pm 1/2\leftrightarrow\pm 3/2$ transition may be narrower than the $\pm 3/2\leftrightarrow\pm 5/2$ transition.

The last point concerns the response of the spin system to circularly polarized rf. For a single crystal in a dc field much larger than the local field, different spectra are observed for the two possible polarizations of circularly polarized rf. This arises because the functions $g_{\pm m}$ are well separated, and have opposite signs. Due to the averaging in the powder, the corresponding functions for the powder sample overlap completely. Thus the line shape is the same when using linearly polarized rf as when using rf of either circular polarization.

C. Determination of quadrupolar parameters

In general one cannot determine e^2qQ/h and η separately, for $\mathbf{I}=3/2$, from pure NQR. For $\mathbf{I}=5/2$, e^2qQ/h and η can be evaluated separately since there are two pure quadrupolar transitions. For both the single crystal and powder samples, the resonances in a small magnetic field are centered about the pure quadrupolar resonance frequencies. For $\mathbf{I}=3/2$, the frequency,

$$\omega_Q=\frac{e^2qQ}{2\hbar}\left(1+\frac{\eta^2}{3}\right)^{1/2} \quad (18)$$

is well known. We find that, for $\mathbf{I}=5/2$, the $\pm 1/2\leftrightarrow\pm 3/2$ transition occurs at

$$\omega_{Q,L}=\frac{e^2qQ}{20\hbar}r(2\sqrt{3})\sin\left(\frac{\theta}{3}\right) \quad (19)$$

while the $\pm 3/2\leftrightarrow\pm 5/2$ transition occurs at

$$\omega_{Q,H} = \frac{e^2qQ}{20\hbar} r\left[3\cos\left(\frac{\theta}{3}\right) - \sqrt{3}\sin\left(\frac{\theta}{3}\right)\right], \quad (20)$$

where

$$r = \left(\frac{7}{3}\eta^2 + 7\right)^{1/2}, \quad (21a)$$

$$\theta = \arctan\left[\frac{-P}{10(\eta^2 - 1)}\right], \quad (21b)$$

and

$$P = \left[\frac{343}{27}\eta^6 + \frac{43}{3}\eta^4 + 543\eta^2 + 243\right]^{1/2}. \quad (21c)$$

The ratio of $(\omega_{Q,H}/\omega_{Q,L})$ is used to determine η, and then e^2qQ/h can be determined using either $\omega_{Q,L}$ or $\omega_{Q,H}$. It appears that these analytical expressions for $\omega_{Q,L}$ and $\omega_{Q,H}$, derived by solving for the roots of the cubic secular equation,[13] have not previously been published.

Using the SQUID NQR technique, spin–lattice and spin–spin relaxation during the rf sweep tend to destroy the symmetry of the line shape for a single sweep. By taking the difference of forward and reverse sweeps, one obtains a line shape that is symmetric with respect to ω_Q. This symmetrization eliminates the need to consider the effects of relaxation when determining ω_Q. Aside from this benefit, the difference spectrum is more immune to instrumental artifacts. This comes about because the NQR signal changes sign when the direction of the rf sweep is reversed, while artifacts generally do not.

III. EXPERIMENT

The applied dc field, usually a few gauss, is trapped in a superconducting lead tube along the laboratory z-axis. A Helmholtz coil along the x-axis provides rf excitation, typically at tens of milligauss levels. In experiments requiring circularly polarized radiation, rf fields which have been phase shifted by 90° are also generated by a similar coil along the y-axis. A Hewlett–Packard 3326A two-channel synthesizer functions as the radio frequency source. The sample is contained in a standard 5 mm NMR tube, attached to the end of a moveable rod. A superconducting pickup coil along the lab z-axis, which is connected to a commercial flux-locked dc SQUID,[14] detects the sample magnetization. The output from the SQUID control unit is digitized and stored on computer. Complete details of the experimental apparatus are available elsewhere.[15,16]

IV. RESULTS

A. Aluminum oxide (α–Al_2O_3, corundum)

α–Al_2O_3 is a dense and highly ordered system in which the oxygen atoms are arranged in a hexagonal closest packed array.[17] Two thirds of the possible aluminum sites, which are all octahedral, are filled in a well defined scheme. Each aluminum nucleus is surrounded by two equilateral triangles of oxygen atoms such that the space group is D_{3d}.[18] This arrangement of oxygen nuclei produces an axially symmetric electric field gradient at the aluminum site, i.e., $\eta = 0$, and the C_3 axis serves as the z-axis of the quadrupolar PAS. The high frequency transitions of single crystal and polycrystalline α–Al_2O_3, recorded with an rf sweep from low to high frequency, are shown in Figs. 2 and 3, respectively. The low and high frequency transitions were observed at 357 ± 3 and 714 ± 3 kHz, giving $e^2qQ/h = 2.38 \pm 0.01$ MHz and $\eta = 0.0 + 0.1$.[9] This is in excellent agreement with earlier work by Pound[1] and others.[19]

B. Petalite ($LiAlSi_4O_{10}$)

In petalite, folded Si_2O_5 layers are linked by Li and Al tetrahedra. The AlO_4 tetrahedra are distorted such that the aluminum–oxygen bond distances are 1.742 and 1.732 Å.[20] The spectrum of petalite is shown in Fig. 4, and the two transitions are determined to be at 834 ± 5 and 1314 ± 5 kHz. Using Eqs. (19)–(21), we find that $e^2qQ/h = 4.56 \pm 0.01$ MHz and $\eta = 0.47 \pm 0.1$. This measurement confirms estimates of e^2qQ/h and η derived from MAS spectra.[21] The relatively broad lines indicate a considerable amount of structural disorder in this natural mineral sample. Dipolar broadening is not expected to contribute significantly to the linewidth.

C. Boron nitride (BN)

Hexagonal boron nitride forms in a layered network of hexagonal rings, similar to graphite.[22] Each ring is made up

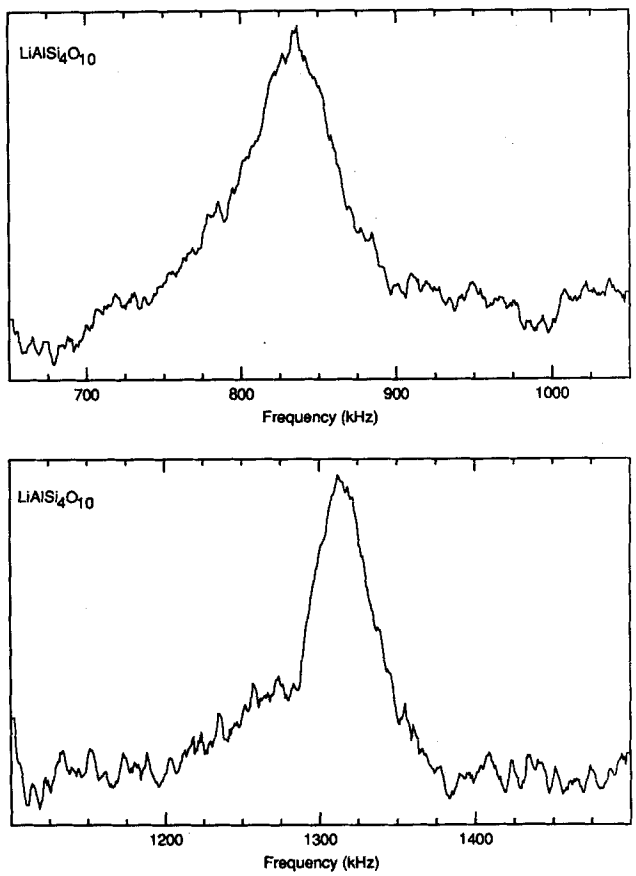

FIG. 4. ^{27}Al NQR powder spectrum of the mineral petalite ($LiAlSi_4O_{10}$), at 4.2 K, derived from the difference between spectra obtained with forward and reverse sweeps of a small rf field, while detecting the dc component of the magnetization with a SQUID. A 10 G dc field was applied to the sample.

of alternating boron and nitrogen nuclei. Directly above and below each boron are the nitrogen nuclei of the adjacent layers. The z-axis of the quadrupolar interaction is perpendicular to the planes formed by the layers. From symmetry considerations, the electric field gradient at the boron nuclei has been taken to be axially symmetric.[23] The spectrum of BN, shown in Fig. 5, has two resonance frequencies, although only one has been previously reported. The position of the high frequency peak, 1467 ± 2 kHz, is in agreement with previous high field results, 1480 ± 50 kHz.[23] We have not yet identified the source of the low frequency shoulder at 1437 ± 2 kHz, but it may be associated with the well-known turbostratic nature of hexagonal boron nitride.[22,24] X-ray diffraction analysis of the BN powder shows that $B_2O_3 \cdot xH_2O$, responsible for the broad peak near 1300 kHz, is the only major crystalline impurity.

D. B_2O_3 and hydrates

The basic units in the borates are planar BO_3 groups and approximately tetrahedral BO_4 groups. The z-axis of the quadrupolar interaction is perpendicular to the plane of the BO_3 group, producing quadrupolar splittings of about 1300 kHz. The undistorted BO_4 group has no electric field gradient at the boron site. Distortions are usually not large enough to bring the quadrupolar splitting of the BO_4 group within the range of our spectrometer. Hence our results are confined to the BO_3 group.

1. $B_2O_3 \cdot 3H_2O$ (boric acid)

The boron nuclei in boric acid are surrounded by three oxygen atoms, in the same plane, such that the O–B–O bond angle is approximately 120°.[25] Although x-ray diffraction and neutron scattering data show two boron sites,[25,26] they do not appear to be resolvable by NQR. The planar BO_3 units are joined together by hydrogen bonding between the oxygen atoms to form a layered network. The signal from boric acid powder is shown in Fig. 6(a). The frequency of the main peak, 1286 ± 5 kHz, is in excellent agreement with the previously reported ^{11}B quadrupole resonance frequency of 1288 ± 4 kHz.[27] Assignment of the high frequency peak, 1335 ± 5 kHz, to the highest frequency transition of ^{10}B is made by comparison with reported ^{10}B resonances at 1335 ± 1 kHz in boric acid enriched with ^{10}B.[27] Further verification of these assignments lay in the absence of the 1335 kHz peak in a sample of 99% ^{11}B-enriched boric acid. A search for the other transitions of the ^{10}B nuclei yielded negative results, leading us to propose that the ^{10}B resonance at 1335 kHz is observable because of spin diffusion between the ^{10}B and ^{11}B nuclear spin systems.[28] This conclusion is supported by the fact that the high frequency transition is not observable while sweeping rapidly from low to high frequency, since the ^{11}B spins are still saturated when the rf reaches the ^{10}B line. A rapid high to low frequency sweep yields a larger ^{10}B line and a reduced ^{11}B line. The small linewidth of the ^{10}B transition relative to the ^{11}B transition may be partially attributed to the quenching of the dipolar interaction in integer spin systems[29] and partially to the reduced Zeeman interaction, due to the smaller magnetic moment of ^{10}B.

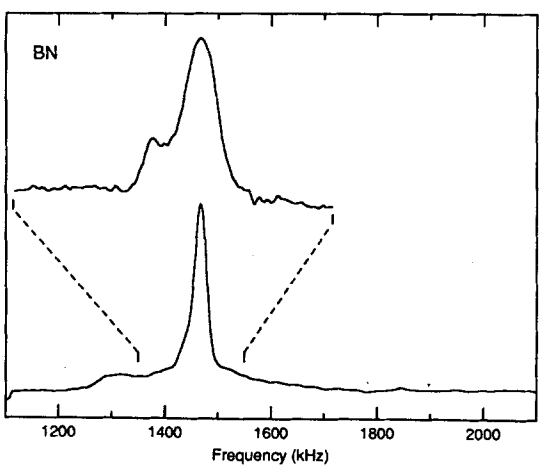

FIG. 5. ^{11}B NQR spectrum of polycrystalline BN at 4.2 K in a 3.5 G dc magnetic field. The broad resonance at 1300 kHz is due to $B_2O_3 \cdot xH_2O$, which is a product of BN hydrolysis in air (Ref. 30). The upper trace shows an expanded view of the 1467 kHz transition in a hot-pressed rod of BN, obtained in a dc field of 1.2 G. No decomposition products were observed in the hot-pressed rod. Both spectra are the difference between spectra obtained with forward and reverse sweeps.

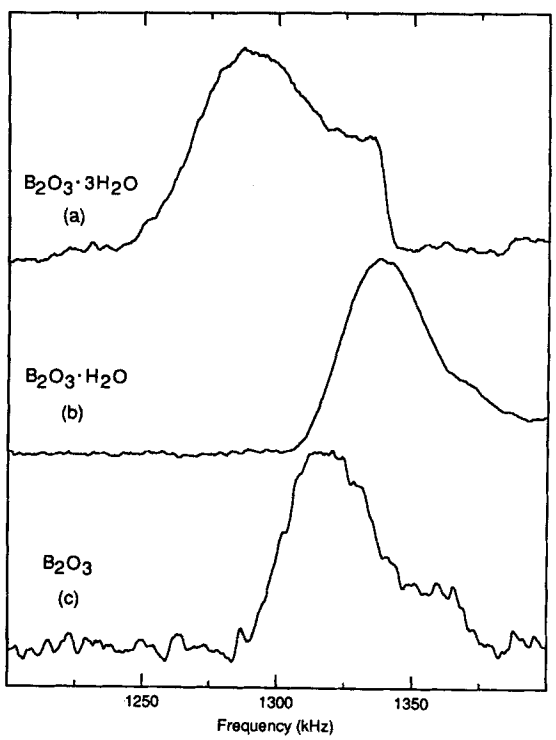

FIG. 6. Boron NQR spectra of polycrystalline borates in a 10 G dc field at 4.2 K. The high frequency shoulders on the main peaks in (a), (b), and (c) are from ^{10}B, arising from spin diffusion between the ^{11}B and ^{10}B spin systems. These spectra are the difference between forward and reverse sweeps.

2. $B_2O_3 \cdot H_2O$(III) (orthorhombic)

This sample was prepared by heating powdered boric acid, in an open container, at 100 °C for 24 h.[30,31] $B_2O_3 \cdot H_2O$ has a layered structure in which B_3O_3 rings are joined by hydrogen bonding between OH groups on the boron atoms.[30,32] The immediate environment of the boron is similar to that in boric acid, except there is a lower extent of hydrogen bonding in $B_2O_3 \cdot H_2O$. Our measured transition frequency from Fig. 6(b), 1338 ± 10 kHz, is significantly different from that obtained from the second order quadrupolar broadening of the Zeeman transition, 1280 ± 10 kHz.[33] The high frequency shoulder on the main resonance is attributed to the $|\pm 2\rangle \leftrightarrow |\pm 3\rangle$ transition of ^{10}B.

3. B_2O_3 (polycrystalline)

The crystalline form of B_2O_3 consists of trigonal BO_3 groups joined through their oxygen atoms to form a three-dimensional network.[32] This sample of polycrystalline B_2O_3, dried overnight at 70 °C, yields a main peak at 1320 ± 10 kHz and a shoulder on the high frequency side at 1360 ± 10 kHz, Fig. 6(c). The separation between the main peak and the shoulder is the same as that observed in boric acid, so we assign the shoulder to the ^{10}B resonance. Previous work on the glass phase of ^{10}B-enriched B_2O_3 shows a ^{10}B transition around 1375 kHz.[4]

4. B_2O_3 (glass)

This sample was prepared by heating boric acid in a graphite mold until bubbling had essentially ceased. The slug of B_2O_3 glass was then extracted from the mold. Vitreous B_2O_3 consists of a three-dimensional network of BO_3 triangles and B_3O_3 rings connected by bridging oxygen atoms.[4,30] The resonance, shown in Fig. 7, occurs at 1360 ± 10 kHz in reasonable agreement with previous work.[4,34] The broad spectrum indicates large variations in the electric field gradients at the boron-11 nuclear sites, as expected from the glassy structure. A measurement of the linewidth is of interest because it is directly related to the distribution in the boron sites. An estimate of the linewidth from the fitting of high-field NMR experiments yielded a width of about 100 kHz (FWHM), while our direct measurement gives only 80 kHz. We may ignore the effect of the small dc magnetic field, which causes a broadening of only 2 or 3 kHz. Recent pure NQR work with a conventional spectrometer gives a linewidth of 60 kHz for vitreous B_2O_3.[35]

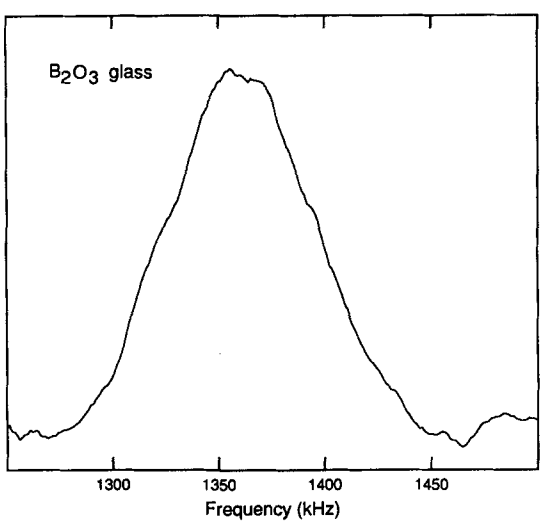

FIG. 7. ^{11}B NQR spectrum of vitreous B_2O_3 at 4.2 K in a dc field of 2.4 G. This spectrum is the difference between forward and reverse sweeps.

V. CONCLUSIONS

Using the low frequency sensitivity of our SQUID spectrometer, we have made several measurements of low frequency NQR of aluminum and boron. ^{27}Al NQR resonances in α–Al_2O_3 and petalite were detected in the range from 350 to 1300 kHz, allowing for easy, accurate determinations of e^2qQ/h and η. The ^{11}B NQR resonances were observed between 1 and 1.5 MHz in boron nitride, polycrystalline $B_2O_3 \cdot xH_2O$, and in vitreous B_2O_3. In addition, the $|\pm 2\rangle \leftrightarrow |\pm 3\rangle$ ^{10}B resonance was observed in polycrystalline $B_2O_3 \cdot xH_2O$ via cross relaxation with the ^{11}B spin system. In most cases, our results compare well with those obtained with conventional techniques, considering the small structural changes expected when cooling to 4.2 K. However, in several samples we were able to obtain more accurate or more detailed spectral information than was previously available. We feel that this technique has very broad applicability in NQR of aluminum, boron, and other nuclei in this frequency range, particularly in disordered systems like glasses and amorphous materials. Efforts are currently underway to extend this technique to other half-odd-integer and $\mathbf{I} = 1$ spin systems.

ACKNOWLEDGMENTS

C. C. was supported by a Natural Sciences and Engineering Research Council 1967 Science and Engineering Scholarship. We thank Professor J. Stebbins of Stanford University for the loan of the petalite sample, and B. Black for assistance in obtaining some of the spectra. This work was supported by the Director, Office of Energy Research, Office of Basic Energy Sciences, Materials Sciences Division of the U.S. Department of Energy and by the Director's Program Development Fund of Lawrence Berkeley Laboratory, under Contract No. DE-AC03-76SF00098.

[1] R. V. Pound, Phys. Rev. **79**, 685(1950); C. H. Townes and B. P. Dailey, J. Chem. Phys. **17**, 782(1949); C. H. Townes and B. P. Dailey, *ibid.* **20**, 35(1952).

[2] M. H. Cohen and F. Reif, in *Solid State Physics*, edited by F. Seitz and D. Turnbull (Academic, New York, 1957), Vol. 5, pp. 321–438; T. P. Das and E. L. Hahn, *Solid State Physics*, Supplement 1, edited by F. Seitz and D. Turnbull (Academic, New York, 1958).

[3] A. Samoson, E. Kundla, and E. Lippmaa, J. Magn. Reson. **49**, 350(1982); E. Kundla, A. Samoson, and E. Lippmaa, Chem. Phys. Lett. **83**, 229 (1981).

[4] G. E. Jellison, Jr., L. W. Panek, P. J. Bray, and G. B. Rouse, Jr., J. Chem. Phys. **66**, 802(1977); P. J. Bray, J. Non-Cryst. Solids **73**, 19(1985).

[5] B. F. Chmelka, K. T. Mueller, A. Pines, J. Stebbins, Y. Wu, and J. W. Zwanziger, Nature **339**, 42(1989).
[6] A. G. Redfield, Phys. Rev. **130**, 589(1963); R. L. Strombotne and E. L. Hahn, Phys. Rev. A **133**, 1616(1964); D. B. Zax, A. Bielecki, K. W. Zilm, A. Pines, and D. P. Weitekamp, J. Chem. Phys. **83**, 4877(1985).
[7] J. Clarke, in *Superconductor Applications: SQUIDs and Machines*, edited by B. B. Schwartz and S. Foner (Plenum, New York, 1977), p. 67; J. Clarke, Proc. IEEE **61**, 8(1973); J. Clarke, Phys. Today **39**, 36(1986).
[8] E. P. Day, Phys. Rev. Lett. **29**, 540(1972); T. Jach, Appl. Phys. Lett. **28**, 49(1976).
[9] J. Chang, C. Connor, E. L. Hahn, H. Huber, and A. Pines, J. Magn. Reson. **82**, 387(1989).
[10] C. Dean, Phys. Rev. **96**, 1053(1954).
[11] M. Bloom, E. L. Hahn, and B. Herzog, Phys. Rev. **97**, 1699(1955); M. J. Weber and E. L. Hahn, *ibid.* **120**, 365(1960).
[12] N. Bloembergen, S. Shapiro, P. S. Pershan, and J. O. Artman, Phys. Rev. **114**, 445(1959).
[13] M. H. Cohen, Phys. Rev. **96**, 1278(1954); T. P. Das and E. L. Hahn, *Solid State Physics*, Supplement 1, edited by F. Seitz and D. Turnbull (Academic, New York, 1958), p. 13. The second equation in Table I, on page 13, should read $E^3 - 7(3 + \eta^2)E - 20(1 - \eta^2) = 0$.
[14] Model DBS DYNABIAS dc SQUID System, Biomagnetic Technologies, Inc., San Diego, CA 92121.
[15] C. Connor, J. Chang, and A. Pines, Rev. Sci. Instrum. **61**, 1059(1990).
[16] C. Connor, Ph.D. thesis, University of California, Berkeley (1989), Lawrence Berkeley Laboratory Report No. LBL-28544.
[17] N. Ishizawa, T. Miyata, I. Minato, F. Marumo, and S. Iwai, Acta Cryst. **B36**, 228(1980).
[18] R. W. C. Wyckoff, *The Structure of Crystals* (Rheinhold, New York, 1935); *Crystal Structures* (Interscience, New York, 1948).
[19] H. J. Jakobsen, J. Skibsted, H. Bildsøe, and N. Chr. Nielsen, J. Magn. Reson. **85**, 173(1989).
[20] T. Tagai, H. Ried, W. Joswig, and M. Korekawa, Z. Kristallogr. **160**, 159(1982).
[21] A. Samoson (private communication).
[22] R. S. Pease, Acta Cryst. **5**, 356(1952).
[23] A. H. Silver and P. J. Bray, J. Chem. Phys. **32**, 288(1960).
[24] J. Thomas, Jr., N. E. Weston, and T. E. O'Connor, J. Am. Chem. Soc. **84**, 4619(1963).
[25] W. H. Zachariasen, Acta Cryst. **7**, 305(1954).
[26] B. M. Craven and T. M. Sabine, Acta Cryst. **20**, 214 (1966).
[27] L. G. Butler and T. L. Brown, J. Magn. Reson. **42**, 120(1981).
[28] D. T. Edmonds, Phys. Rep. **29**, 233(1977); D. T. Edmonds, Int. Rev. Phys. Chem. **2**, 103(1982).
[29] G. W. Leppelmeier and E. L. Hahn, Phys. Rev. **141**, 724(1966).
[30] F. A. Cotton and G. Wilkinson, *Advanced Inorganic Chemistry*, 4th ed. (Wiley, New York, 1980).
[31] P. H. Kemp, *The Chemistry of Borates*, Part I (Borax Consolidated Ltd., London, 1956).
[32] N. N. Greenwood and A. Earnshaw, *Chemistry of the Elements* (Pergamon, New York, 1984).
[33] A. H. Silver, J. Chem. Phys. **32**, 959(1960).
[34] P. W. France and M. Wadsworth, J. Magn. Reson. **49**, 48(1982); G. L. Turner, K. A. Smith, R. J. Kirkpatrick, and E. Oldfield, *ibid.* **67**, 544(1986).
[35] P. J. Bray, Bull. Am. Phys. Soc. **34**, 900(1989).